TABLE 1 Comparison of the Computed Stop Band With Reported TRM, FEM, and Measurements [2]

	TRM	FEM	Measurements	Analytical Model
f_{start} (GHz)	3.13	1.898	1.9	2.05
f_{stop} (GHz)	5.34	5.28	5.25	5.60
Bandwidth (GHz)	2.21	3.382	3.35	3.55

mm,50 mm) and (90 mm,50 mm). There is an eight-unit cell separation between the two ports.

In this board, the truncation of the patch corner reduces the patch capacitance. Considering the truncated area, the patch capacitance is modified to

$$C = \frac{\varepsilon_0 \varepsilon_{r2}(s^2 - \text{Area}_{\text{trunct}})}{t_2}. \quad (11)$$

For this case, (20,20) modes are used for (X,Y) directions in calculation. The analytical model-predicted 20-dB bandgap is from 2.0 to 5.6 GHz, as seen in Figure 3. In Ref. 2, several methods including transverse resonance method (TRM) and finite element method (FEM) simulations results and measured data were presented. The comparisons between results computed by the analytical model in the study and the results reported in Ref. 2 are listed in Table 1.

Case 2 is a power plane, which consists of a set of EBG patches sandwiched in the substrate reported in Ref. 6. The calculated results are shown in Figure 4. The overall board height $h = 2.84$ mm (112 mil), $a = 0.51$ mm (20 mil), $d = 8.00$ mm (315 mil), $g = 0.76$ mm (30 mil), $s = 7.24$ mm (285 mil), $t1 = 2.36$ mm (93 mil), $\varepsilon_{r1} = 4.3$, and $\varepsilon_{r2} = 4.0$. In the reported Etenna's board, the overall board dimension is 191×140 mm^2 with two ports located at (31.8 mm,74.6 mm) and (127.0 mm,7.46 mm). There are 11 unit cells between two ports. For this calculation, (20,20) modes are used for (X,Y) directions too. The measurement data and transmission line circuit-model (TLC) results reported in Ref. 6 are listed in Table 2.

For both cases, the results show that the analytical model-computed stop band agrees well with the measurements (within 10% error). Comparing to the stop band calculated by other two methods (TRW and TLC), less band shift is found in the results predicted by this model.

5. CONCLUSION

In this study, a cavity-based modal analysis model is developed to analyze the EBG characteristics embedded in PCB power plane for power plane noise suppression. By obtaining the currents flowing through the EBG equivalent circuits, thanks to the modal voltage in a bare power plane, the EBG impacts on the total modal voltage can be superposed to the original distribution and the total voltage distribution of the system with EBG patches added may be theoretically derived. This analytical model is validated by the measurement data reported in literature.

TABLE 2 Comparison of the Computed Stop Band With TLC Model and Measurements [6]

	TLC Model	Measurements	Analytical Model
f_{start} (GHz)	2.0	1.5	1.5
f_{stop} (GHz)	5.6	5.4	5.6
Bandwidth (GHz)	3.6	3.9	4.1

REFERENCES

1. I. Novak, Reducing simultaneous switching noise and EMI on ground/power planes by dissipative edge termination, IEEE Trans Compon Packag Manuf Technol 22 (1999), 274–283.
2. R. Abhari and G.V. Eleftheriades, Suppression of the parallel-plate noise in high speed circuits using a metallic electromagnetic band-gap structure, IEEE International Microwave Symposium Digest, June 2–7, 2002, Seattle, WA, pp. 493–496.
3. T. Kamgaing and O.M. Ramahi, High-impedance electromagnetic surfaces for parallel-plate mode suppression in high speed digital systems, IEEE 11th Topical Meeting on Electrical Performance of Electronic Packaging, Monterey, CA, October 21–23, 2002, pp. 279–282.
4. S. Rogers, X. Wu, A. Waltho, and D. Xu, Noise reduction in digital/RF daughter card with electromagnetic bandgap layers, IEEE 13th Topical Meeting on Electrical Performance of Electronic Packaging, Portland, OR, October 25–27, 2004, pp. 203–206.
5. S. Shahparnia and O.M. Ramahi, A simple and effective model for electromagnetic bandgap structures embedded in printed circuit boards, IEEE Microw Wireless Compon Lett 15 (2005), 621–623.
6. S.D. Rogers, Electromagnetic-bandgap layers for broad-band suppression of TEM modes in powerplanes, IEEE Trans Microw Theory Tech 53 (2005), 2495–2505.
7. G. Lei, R.W. Techentin, P.R. Hayes, D.J. Schwave, and B.K. Gilbert, Wave model solution to the ground/power plane noise problem, IEEE Trans Instrum Meas 44 (1995), 300–303.
8. X. Wu, A wave model for EBG in power plane noise mitigation, presented at the Proceedings of IEEE APS-URSI Symposium, Albuquerque, NM, July 9–14, 2006.
9. M. Hampe and S. Dickman, Improving the behavior of PCB power-bus structures by an appropriate segmentation, presented at the Proceedings of International Symposium on Electromagnetic Compatibility, Chicago, IL, August 2005; Vol. 3, no. 8–12, pp. 961–966.
10. M. Lai, J.-F. Kiang, and S.-K. Jeng, Multi-layered PCB power plane resonance analysis using method of lines, presented at the Proceedings of 14th International Zurich Symposium and Technical Exhibition on Electromagnetic Compatibility, Zurich, Switzerland, February 20–22, 2001, pp. 265–268.

ALL-OPTICAL ON–OFF SWITCH BASED ON BISMUTH-BASED HIGHLY NONLINEAR FIBER

K. K. Qureshi,[1,2] P. K. A. Wai,[1,3] H. Y. Tam,[1,2] L. Chao,[1,3] and N. Sugimoto[4]

[1] Photonics Research Center, The Hong Kong Polytechnic University, Hong Kong, China
[2] Department of Electrical Engineering, The Hong Kong Polytechnic University, Hong Kong, China
[3] Department of Electronic and Information Engineering, The Hong Kong Polytechnic University, Hong Kong, China
[4] Asahi Glass Co., Ltd, 1150 Hazawa-cho, Yokohama 221-8755, Japan

Received 7 September 2006

ABSTRACT: *We propose a simple and compact all-optical on–off switch working at 10 Gb/s. The operation of the switch is based on four-wave mixing in only 1.9 m of bismuth-based highly nonlinear fiber. The proposed switch has a fast response time, high ON/OFF switching ratio, and potential to work beyond 10 Gb/s.* © 2007 Wiley Periodicals, Inc. Microwave Opt Technol Lett 49: 838–841, 2007; Published online in Wiley InterScience (www.interscience.wiley.com). DOI 10.1002/mop.22295

Key words: *all-optical switch; nonlinear optics; optical fiber devices*

1. INTRODUCTION

Optical networks utilizing fast packet switching are expected to provide the required capacities and flexibility in the next generation high-speed optical networks [1]. An all-optical switch will be one of the key component in future high capacity optical networks. Hitherto, a variety of switching schemes have been reported and demonstrated [1–6]. Nonlinear optical fiber loop mirror (NOLM), pioneered by Doren and Wood [2], is a Sagnac interferometer that makes use of cross-phase modulation (XPM) for optical switching. It can switch pulses that are several femto-second long. However, NOLM-based devices require long interaction lengths, which makes the overall system very bulky. In addition, their operation suffers from the signal polarization dependence and careful control is needed to ensure their stable operation. A switching scheme based on self-induced gain modulation (SGM) in the cascaded SOA configuration by counter propagating the data and control signals has been demonstrated [5]. The scheme offers large extinction ratio but the switching scheme is limited. Ultrafast switching based on four-wave mixing (FWM) in polarization maintaining fiber loop has been reported in a number of studies [6–8]. Performance of the scheme is mainly limited by its low efficiency due to limited nonlinearity of available fiber. This means long length of fiber is often needed and phase-matching condition is often compromised.

In this letter, we propose an all-optical on–off switch based on FWM using only 1.9 m of bismuth-based highly nonlinear fiber (Bi-HNLF) (courtesy of Asahi Glass). The control and data signals together are launched into the Bi-HNLF, which serves as the all-optical on–off switch. When the control signal is high, i.e. the ON state, the data signal will be switched onto the idlers generated by the FWM effect. When the control signal is low, i.e. the OFF state, no idlers will be generated. The data signal will therefore not be switched. As a result, the data signals will be switched onto the new wavelength depending on the states of the control signals. With the large nonlinear coefficient and short length of the fiber, high efficiency can be obtained.

2. EXPERIMENTAL RESULTS AND DISCUSSIONS

Figure 1 shows the FWM conversion efficiency of 1.9-m long Bi-HNLF, which is defined as the ratio of the output wavelength converted signal power to the input signal power as a function of signal wavelength detuning relative to the fixed pump wavelength. In this experiment, the pump wavelength is kept fixed at 1550 nm. A maximum conversion efficiency of −16.8 dB is achieved with a 3-dB bandwidth of ~10 nm. The conversion-bandwidth limit of ~10 nm can be attributed to the walk-off effect caused by the GVD, which still remained in spite of the short fiber length. Because of the extremely high material dispersion of the Bismuth glass, the GVD control for the Bi-HNLF is not achieved in a straightforward manner unless a special waveguide structure such as photonic crystal fiber structure is employed [9].

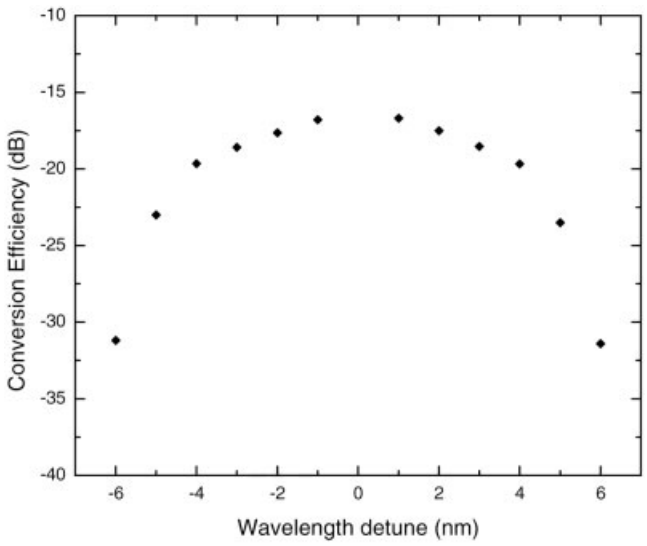

Figure 1 Measured conversion efficiency versus signal wavelength detuning relative to fixed pump wavelength of 1550 nm

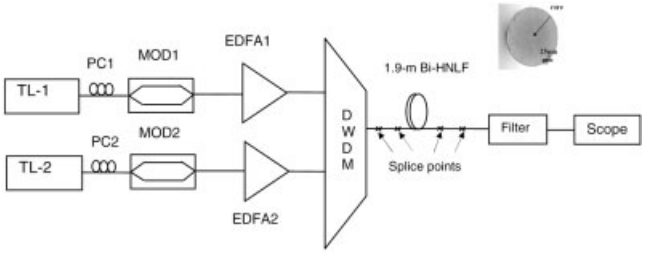

Figure 2 Experimental setup of the all-optical Bi-HNLF based on–off switch. TL: Tunable laser; PC: Polarization controller; MOD: Modulator; EDFA: Erbium-doped fiber amplifier; DWDM: Dense wavelength division multiplexer

Figure 2 shows the schematic of the experimental setup to demonstrate the proposed all-optical on–off switching using Bi-HNLF. The data signal at 1553.33 nm is encoded by $2^{31} - 1$ nonreturn-to-zero pseudorandom bit patterns at 10 Gb/s. The data signal is generated by externally modulating a tunable laser (TL-1) with an electro-optic lithium niobate ($LiNbO_3$) modulator driven by a 10 Gb/s pulse pattern generator. The control signal at 1554.13 nm was generated by external modulation of another tunable laser (TL-2). The wavelength separation between the control and data signals is chosen to be 0.8 nm, so that the idlers wavelength will be placed 0.8 nm apart. The data and the control signals were amplified separately to an average power of about 300 mW by using erbium-doped fiber amplifiers (EDFAs), which have maximum saturation output power of 500 mW. Polarization controllers (PCs) were used to ensure coincidence of the states-of-polarization of the control and data signals. The data and control signals were combined in an 8-channel DWDM multiplexer and then launched into 1.9 m of Bi-HNLF.

The mode field diameter (MFD) and the effective core area A_{eff} of the Bi-HNLF are estimated to be 2.1 μm and 3.3 μm^2, respectively. If direct fusion-splicing of the Bi-HNLF to SMF28 is done, the splicing loss would be very large because of large MFD mismatch (Bi-NLF: 2.1 μm, SMF: 10.4 μm). Hence, to reduce splicing losses, the two ends of the Bi-HNLF are first connected to two segments of ultra high numerical aperture (NA) silica fiber (UHNA4, Nufern), which has a mode field diameter (MFD) of 4 μm. The two high NA fibers are then connected to conventional silica fiber (SMF28), which has a MFD of 10.4 μm. These fibers are fusion-spliced by arc discharge using a conventional fusion splicing machine. The total loss at the input side of the Bi-HNLF, which includes the splice loss between the SMF28 and UHNA4, the splice loss between the UHNA4 and the Bi-HNLF, and the propagation losses in the SMF28 and the UHNA4, is 1.1 dB. The total loss at the output side of the Bi-HNLF is 2.6 dB. The propagation loss of the Bi-HNLF is 2.0 dB/m at 1550 nm. The total loss of the Bi-HNLF is therefore 7.5 dB. The refractive index of the core and cladding are 2.22 and 2.13, respectively. Thus the numerical aperture of this fiber is 0.64. The group velocity disper-

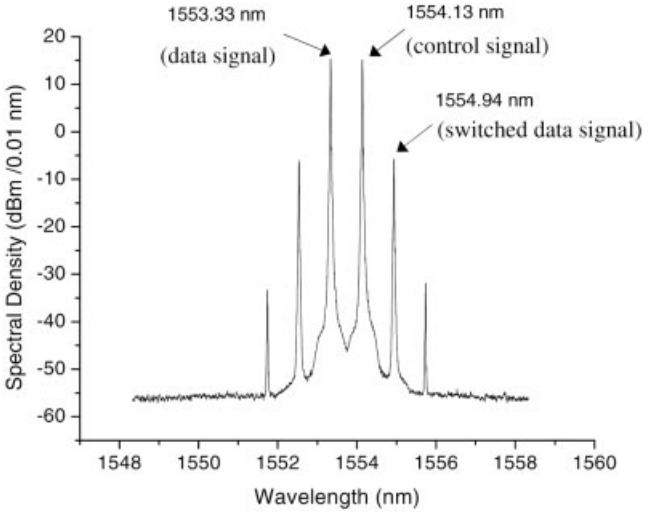

Figure 3 Output spectra of FWM signals

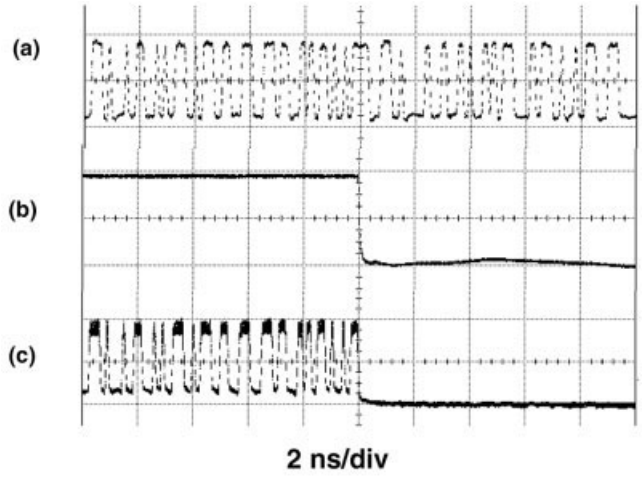

Figure 5 Magnified timing diagrams of (a) 10 Gb/s NRZ data signal at 1553.33 nm, (b) synchronized control signal with 64 ns on-off duration at 1554.13 nm, and (c) switched 10 Gb/s data signal 1554.94 nm

sion (GVD) and the nonlinearity coefficients of the Bi-HNLF at 1550 nm are -280 ps/nm/km and 1000 W^{-1} km^{-1}, respectively. The nonlinearity coefficient of this fiber is $\sim$100 times larger than that of the conventional silica-based highly nonlinear dispersion-shifted fiber. Although the Bi-HNLF has a large normal GVD coefficient, which is mainly due to the material dispersion of the high refractive index glass, its effect however is not significant because of short fiber length used. Figure 3 shows the spectra of FWM signals measured at the output of the Bi-HNLF. Multiple wavelengths generated by the FWM process are observed. The newly generated wavelengths are 0.8 nm apart and they all carry the switched data. We used a thin film filter with a bandwidth of 0.6 nm to filter out the switched signal. The output is observed using an optical spectrum analyzer with 0.01 nm resolution and a 50 GHz sampling oscilloscope. Figures 4(a) and 4(b) depict the timing diagrams of the data and control signals, respectively. The control signal has an ON/OFF duration of 64 ns. The portion of data signal, which coincides with the ON duration of the control signal, will be switched and wavelength-converted by the FWM process, whereas the portion of the data signal, which coincides with the OFF period will be blocked. Figure 4(c) shows the timing diagram of the switched data signal at 1554.94 nm. Figure 5 depicts the magnified timing diagrams of Figure 4. The switched data has a relatively low noise level and high extinction ratio. The proposed on–off switch therefore can potentially operate at speed beyond 10 Gbit/s. The Figures 6(a) and 6(b) show the eye diagrams of the input data signal and the switched data signal, respectively. Clear eye opening and no pattern-dependent effect of the switched signal is observed. The thickness of the "1" rail is due to the beating between the in-band ASE of the two EDFAs, which transferred to the idlers.

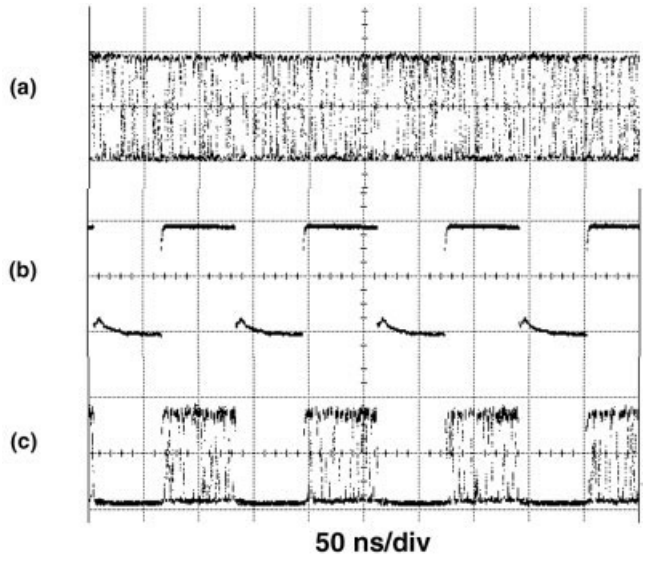

Figure 4 Timing diagrams of (a) 10 Gb/s NRZ data signal at 1553.33 nm, (b) synchronized control signal with on–off duration of 64 ns at 1554.13 nm, and (c) switched 10 Gb/s data signal at 1554.94 nm

3. CONCLUSION

In conclusion, we have experimentally demonstrated all-optical on–off switching at 10 Gb/s based on four-wave mixing using only 1.9 m of bismuth-based highly nonlinear fiber. The demonstrated on–off switch has a fast response time, and the switched signal shows a high extinction ratio. The proposed on–off switch can potentially operate at speeds beyond 10 Gb/s.

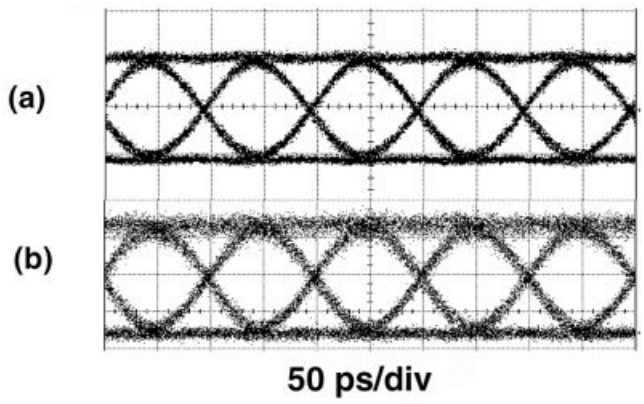

Figure 6 Eye diagrams of the (a) input data signal and (b) switched data signal

ACKNOWLEDGMENTS

This research is supported in part by grants from The Hong Kong Polytechnic University (Project Number A-PG60 and G-U155).

REFERENCES

1. L.Y. Chan, P.K.A. Wai, L.F.K. Lui, B. Moses, W.H. Chung, H.Y. Tam, and M.S. Demokan, Demonstration of an all optical switch by use of a multiwavelength mutual injection-locked laser diode, Opt Lett 28 (2003), 837–839.
2. N.J. Dorren and D. Wood, Nonlinear optical loop mirror, Opt Lett 13 (1988), 56–58.
3. K.L. Blow, N.J. Dorren, and B.P. Nelson, Demonstration of the nonlinear loop mirror as an ultrafast all-optical demultiplexer, Electron Lett 26 (1990), 962–964.
4. H.C. Lim, T. Sakamoto, and K. Kikuchi, Polarization independent optical demultiplexing by conventional nonlinear optical loop mirror in a polarization diversity loop configuration, IEEE Photon Technol Lett 12 (2000), 1704–1706.
5. J.H. Kim, K. R. Oh, H.S. Kim, and K. Chao, All-optical switching by counter propagating operation in cascaded semiconductor optical amplifiers, IEEE Photon Technol Lett 12 (2000), 513–515.
6. T. Morioka, S. Kawanishi, K. Uchiyama, H. Takara, and M. Saruwatari, Polarisation-independent 100 Gbit/s all-optical demultiplexer using four-wave mixing in a polarisation-maintaining fibre loop, Electron Lett 30 (1994), 591–592.
7. P.O. Hedekvist and P.A. Andrekson, Demonstration of fibre four-wave mixing optical demultiplexing with 19 dB parametric amplification, Electron Lett 32 (1996), 830–831.
8. K. Kikuchi and C. Lorattanasane, Design of highly efficient four-wave mixing devices using optical fibers, IEEE Photon Technol Lett 6 (1994), 992–994.
9. H. Ebendorff-Heidepriem, P. Petropoulos, S. Asimakis, V. Finazzi, R.C. Moore, K. Frampton, F. Koizumi, D.J. Richardson, and T.M. Monro, Bismuth glass holey fibers with high nonlinearity, Opt Express 12 (2004), 5082–5087.

TUNABLE FLAT-TOP FIBER BRAGG GRATING FILTERS FABRICATED IN HYDROGEN-LOADED GRADED-INDEX MULTIMODE FIBERS

Hong-Yan Fu, Wei-Sheng Liu, and Li-Yang Shao
Centre for Optical and Electromagnetic Research, Zhejiang University, Joint Research Center of Photonics of the Royal Institute of Technology (Sweden) and Zhejiang University, East Building No.5, Zijingang Campus, Zhejiang University, Hangzhou 310058, China

Received 11 August 2006

ABSTRACT: *We propose an experimental realization of flat-top filters by fabricating fiber Bragg gratings in graded-index multimode fibers (GI-MMF). Two types of GI-MMFs were used to make this kind of filters, and their spectra and polarization properties were experimentally investigated.* © 2007 Wiley Periodicals, Inc. Microwave Opt Technol Lett 49: 841–843, 2007; Published online in Wiley InterScience (www.interscience.wiley.com). DOI 10.1002/mop.22286

Key words: *fiber optics communication; fiber Bragg grating; multimode fiber; optical fiber*

1. INTRODUCTION

Fiber Bragg gratings (FBGs) are playing an important role in many applications [1], e.g. spectrum filtering, dispersion compensation, fiber lasers and sensors. FBGs in single mode fiber (SMF) have been extensively studied during the past decades. Recently, FBGs in multimode fiber (MMF) have attracted much attention due to their advantages of easy coupling efficiency with the light source and the ease of fabrication (since the growth of FBGs in MMF is faster than that in SMF [2]). Moreover, the graded-index MMF (GI-MMF) has relatively low dispersion and is suitable for optical communication. So far, theoretical analysis of FBGs in MMF can be carried out with the coupled mode theory (CMT) [3] and many devices based on FBGs in MMF have been developed, such as the microbending and temperature sensor [4] and narrow band high-reflectivity filters based on the FBG fabricated in a novel step-index MMF [5].

Meanwhile, filters with flat-top spectral response are desirable components in optical communication systems. Many flat-top filters have been proposed, most of which are realized by either fabricating strong gratings or designing gratings with complicated structures [6]. In this study, we propose and demonstrate flat-top filters by fabricating FBGs in hydrogen-loaded GI-MMFs. Because of the specifically designed index profile of the GI-MMF, a number of modes with close propagation constants couple with each other, and the overlapping of the coupling results in the flat-top filter. Two types of GI-MMFs are employed to fabricate the proposed flat-top filters. FBGs with different index modulation depth are achieved in both types of GI-MMFs, and their spectral characteristics are compared. The utmost flat-top bandwidth of 0.6 nm is achieved with the FWHM of about 0.8 nm. In our experiment, we have shown that the filter is insensitive to the variation of the polarization state. Also, the proposed filter has a larger tunable range than that fabricated in SMF. Compared to the flat-top filters based on FBGs in SMF (SMFBG), the proposed filter is easier to be fabricated and possesses relatively larger tunability.

2. EXPERIMENTAL RESULTS AND ANALYSIS

We fabricated FBGs in two different kinds of GI-MMFs with the phase mask technique by our point-by-point auto-fabrication system. An optical spectrum analyzer (OSA) was utilized to measure the transmission and reflection spectra of FBGs. The period of the phase mask is1070.6 nm. The first type of GI-MMF used here was the commercial GI-MMF (made by Corning) with a core diameter (cladding diameter) of 62.5 μm (125 μm). The second type of GI-MMF is another kind of commercial fiber (Model: 100/140–24-HTA), whose core diameter (cladding diameter) is 96 μm (130 μm). The maximum reflective index of the fiber core and the reflective index of the cladding are 1.4781 and 1.4585, respectively. The fibers were hydrogen-loaded for 2–3 days at a pressure of 6 MPa and a temperature of 110°C.

The first group of FBGs are fabricated in the Corning MMF (MMFBG-I). The length of the gratings is about 8 mm. The measured reflection spectra with different modulation degree are shown in Figure 1, when 1000 (solid line), 2000 (dotted line), and 3000 (dot dashed line) exposure pulses of the excimer laser are ignited in the fabrication of FBGs. From Figure 1, one can see that as the exposure degree increases, the top of the FBG spectrum is becoming more flat, together with the increase of the flat-top bandwidth, which is determined by the inherent property of the multimode fiber and the hydrogen concentration. This is because more modes with close propagation constants are involved in the mode coupling. In our experiments, with the exposure of 3000 pulses, we got a flat-top filter with the flat-top bandwidth of 0.6 nm and FWHM of over 0.8 nm.

Utilizing the same technique, we also fabricated another group of FBGs in the second type of the GI-MMF (MMFBG-II) with